Single-vortex dynamics in overdamped Josephson junction ladders

1996 J. Phys.: Condens. Matter 8 7463

(http://iopscience.iop.org/0953-8984/8/40/011)

J. Phys.: Condens. Matter **8** (1996) 7463–7472. Printed in the UK

Single-vortex dynamics in overdamped Josephson junction ladders

J C Ciria† and C Giovannella†‡

† Dipartimento di Fisica, and Sezione INFN dell'Università di Roma Tor Vergata, Via della Ricerca Scientifica 1, I-00133 Roma, Italy

‡ Sezione INFM dell'Università di Roma Tor Vergata, Via della Ricerca Scientifica 1, I-00133 Roma, Italy

Received 26 March 1996, in final form 5 June 1996

Abstract. The single-vortex dynamics in ladders of overdamped Josephson junctions is investigated by means of numerical simulations. We derive the velocity (v), the coefficient of viscosity (η) and the height of the dynamical barrier for the cell-to-cell vortex motion (E_b) as functions of the bias current (i_{dc}), the magnetic field penetration depth ($\lambda_\perp$) and the vortex position (x). The vortex dynamics can be satisfactorily described in terms of the motion of a particle subjected to a potential $U(x, i_{dc}, \lambda_\perp)$, the form of which is analysed.

1. Introduction

The dynamical properties of Josephson junction arrays have been extensively studied in the past by several groups, both theoretically and experimentally. The efforts have been mainly centred on the steady dynamical states and their dependence on the external magnetic field, the bias current, the array disorder, the screening field induced by the circulating currents, etc [1].

An appealing subject within this framework is that of vortex dynamics, which has been the object of numerical, analytical and experimental research in recent years. In most cases this study has been performed in the context of the sine–Gordon model, either in its continuous or discrete version that describe, respectively, a long extended junction and a 1D array of parallel shunted junctions [2].

In this paper we present a detailed study of the single-vortex dynamics in a ladder of resistively shunted overdamped Josephson junctions, described by the RSJ model. This study is quite relevant for the practical implementations of devices based on superconducting junction arrays. Indeed, the controlled transmission of localized and quantized excitations (vortices/antivortices) is the operational basis of almost all of the cryoelectronic devices (rapid single-quantum flux logics, neural networks, transistors, photofluxonic detectors, etc) [3]. Indeed, a quantitative study of the processes of creation and propagation of the signals is essential for the design of such kinds of device. One needs to know determinant factors like the velocity of transmission of the vortex/antivortex, and the scales of energy involved in the processes and their dependence on the physical parameters—either external (e.g. the bias current supplied to the circuit, i_{ext}) or intrinsic to the array (i.e. the penetration depth of the magnetic field, $\lambda_\perp$).

We have studied dynamical quantities such as the vortex velocity, v, the coefficient of viscosity, η, and the height of the dynamical barrier for the cell-to-cell vortex motion, E_b.

0953-8984/96/407463+10$19.50

Their dependence on the vortex position (x), the bias current (i_{dc}) and the screening field (parametrized by $\lambda_\perp$) has been carefully worked out.

The dynamics of a single vortex in a ladder can be described in terms of the motion of a particle subjected to a 1D potential $U(x, i_{dc}, \lambda_\perp)$, the shape of which will be discussed in detail. The above-mentioned dynamical quantities can be satisfactorily derived from this potential.

2. The model

For our studies we consider an ordered ladder with square plaquettes and one superconducting junction per link. The dynamics of the ladder is simulated in the limit of zero shunt capacity. We also assume that the phase of the order parameter ϕ_i is constant on each grain (i.e. we consider point grains). The dynamical equations at $T = 0$ are [4]

$$\sum_j \frac{\overline{h}}{2eR_{ij}} \frac{\mathrm{d}}{\mathrm{d}t}(\phi_i - \phi_j - A_{ij}) = \sum_j I_c \sin(\phi_i - \phi_j - A_{ij}) + I_i(\mathrm{ext}) \tag{1}$$

where i, j stand for nearest-neighbour points. $I_i(\mathrm{ext})$ is the external current entering the site i, R_{ij} is the shunt resistance of the junction, and I_c is the critical current. In general, A_{ij} includes the contributions of both the external and the internal magnetic fields:

$$A_{ij} = \frac{2\pi}{\Phi_0} \int_i^j (\boldsymbol{a}_{ext} + \boldsymbol{a}_{int})\ \mathrm{d}\boldsymbol{r} \tag{2}$$

where $\boldsymbol{a}$ is the potential vector, and Φ_0 the flux quantum. In this paper the external magnetic field is set to zero, and A_{ij} is entirely due to the currents circulating in the array (i_{ij}):

$$A_{ij} = \frac{1}{4\pi\lambda_\perp} FF_{ij;kl} i_{kl}. \tag{3}$$

Here FF is the inductance matrix. We have obtained it by applying the Biot–Savart law so as to calculate the magnetic field induced on a link by all of the currents circulating in the array (every current is supposed to flow within a cylinder of length a and radius $0.005a$) [5]. $\lambda_\perp$ is the penetration depth of the magnetic field, defined as in [6]:

$$\lambda_\perp = \frac{1}{2\pi} \frac{\Phi_0}{\mu_0 I_c a} \tag{4}$$

where a is the lattice spacing. We have chosen the gauge

$$\boldsymbol{\nabla} \cdot \boldsymbol{A} = 0 \tag{5}$$

where $\boldsymbol{\nabla}$ is the discrete divergence operator ($(\boldsymbol{\nabla} \cdot \boldsymbol{A})_i = \sum_j A_{ij}$). With this choice, equation (1) becomes

$$\frac{\mathrm{d}}{\mathrm{d}t}\phi_i = G^{-1}_{ij}\left(\sum_l I_c \sin(\phi_j - \phi_l - A_{jl}) + I_j(\mathrm{ext})\right) \tag{6}$$

where the matrix G is the discrete version of the laplacian operator. If the values of the ϕ'_i and A'_{ij} are known at a time t_n, obtaining $\phi_i(t_{n+1})$ is straightforward.

On the other hand, it is well known that any vector field can be decomposed into two components, with zero divergence and curl respectively. The term $(\mathrm{d}/\mathrm{d}t)(A_{ij})$ can be calculated as

$$\frac{\mathrm{d}}{\mathrm{d}t}(A_{ij}) = \overline{FF}^{-1}_{ij;kl} P_1(\phi_k - \phi_l - I_c \sin(\phi_k - \phi_l - A_{kl})) \tag{7}$$

where $\overline{FF}$ is the restriction of FF to the subspace with zero divergence and P_1 is the projection operator onto this subspace. For an $n_x \times n_y$ array, G and $\overline{FF}$ are, respectively, $(n_x \times n_y)^2$ and $((n_x - 1) \times (n_y - 1))^2$ matrices.

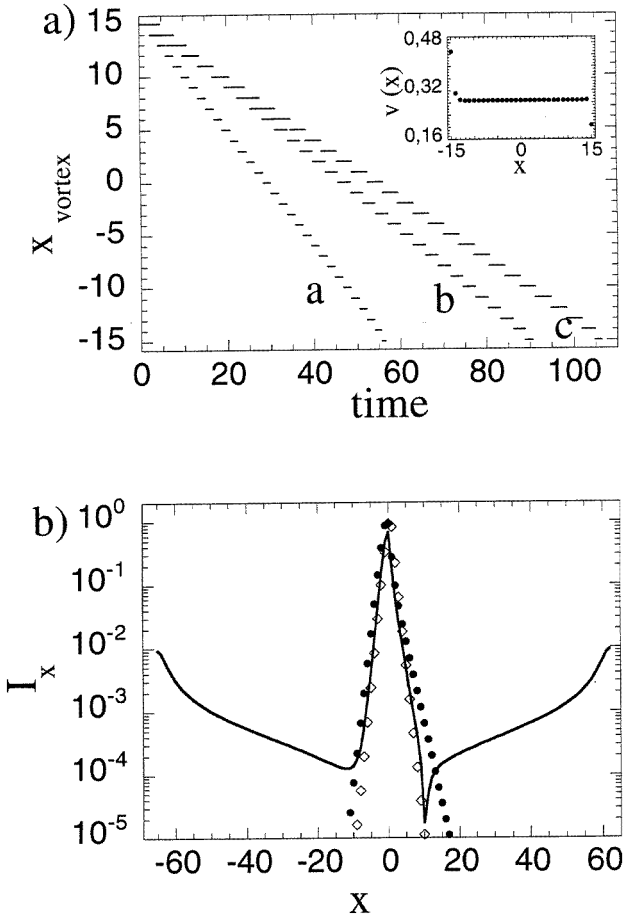

Figure 1. (a) Vortex trajectories in a 32-cell ladder. We consider different values of the parameters: a: $i_{dc} = 0.9$, $\lambda_\perp = \infty$; b: $i_{dc} = 0.9$, $\lambda_\perp = 1$; c: $i_{dc} = 0.7$, $\lambda_\perp = \infty$. The spatial coordinate x and the time are given, respectively, in units of the lattice spacing a and $\tau = \hbar/(2eI_cR_{ij})$. The inset shows the cell-average velocity in case c. (b) The distribution of the horizontal currents (i_x) along the upper branch of a 128-cell ladder, in the cases where $i_{dc} = 0.9$, $\lambda_\perp = \infty$ (black dots), $i_{dc} = 0.5$, $\lambda_\perp = \infty$ (rhombs) and $i_{dc} = 0.9$, $\lambda_\perp = 1$ (continuous line). The distribution is asymmetric because the vortex is in motion (from right to left). Note that the variation of the parameters hardly affects the vortex shape around its centre. The effect of the ladder inductance is to increase the 'peripheral' currents (i.e., the current tends to flow along the external links); in the absence of vortices, i_x is at its maximum at the border. This explains the shape of i_x in the case where $\lambda_\perp = 1$.

It is worthwhile noting that, if the approximation of considering grain points is made, the fluxoid quantization is automatically fulfilled:

$$\sum_{ij\in\alpha} \theta_{ij} + \frac{2\pi}{\Phi_0}(f_\alpha^{tot}) = 2n_\alpha\pi \tag{8}$$

where $\sum_{ij\in\alpha}$ stands for the clockwise sum along the links of the α-plaquette and θ_{ij} is the gauge-invariant phase along the link ij—restricted to the interval $(-\pi, \pi]$–. $f_\alpha^{tot} = \sum_{ij\in\alpha} A_{ij}$ is the total flux through the cell.

The ladder is biased with an external dc current, $I_{ext} = I_{dc}$, that is perpendicular to the ladder. Time is measured in units of the adimensional quantity t/τ, with $\tau = \hbar/(2eI_cR_{ij})$. Currents are normalized to I_c.

The creation of a single vortex is achieved through the temporary breaking of a link at the border of the ladder. The current tends to surround this defect, and vorticity is induced in the rightmost plaquette. After its creation the vortex, subjected to the Lorentz force, moves along the ladder.

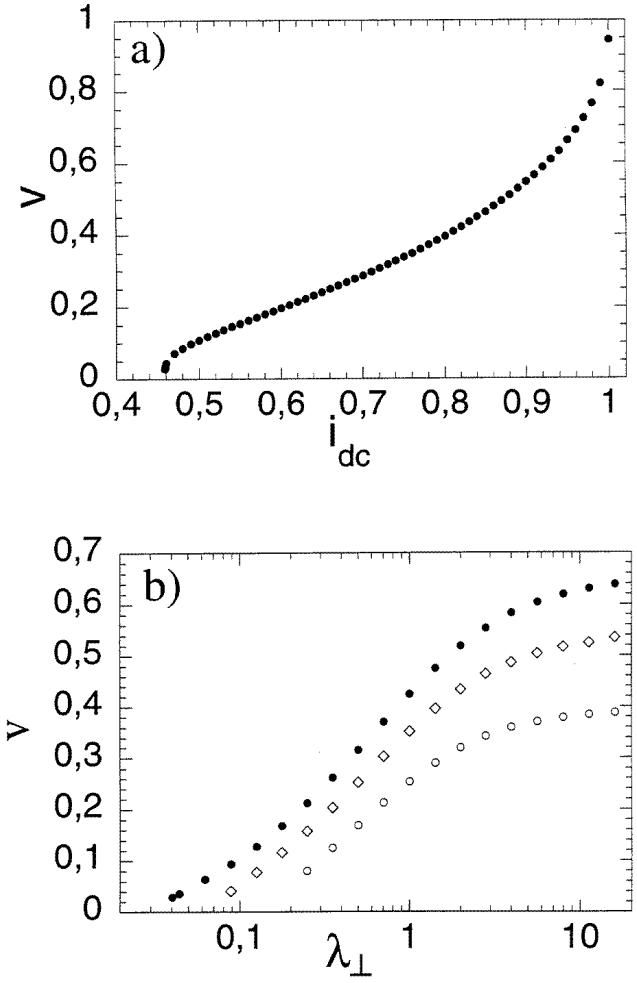

Figure 2. A 64-cell ladder: (a) v versus i_{dc} (infinite penetration depth); (b) v versus $\lambda_\perp$ for $i_{dc} = 0.95$ (black dots), $i_{dc} = 0.90$ (rhombs) and $i_{dc} = 0.80$ (open circles). The values of v plotted refer to the vortex motion far from the border of the ladder (they correspond to the v-plateau shown in the inset of figure 1). v is given in units of a/τ, where a is the lattice spacing and $\tau = \hbar/(2eI_cR_{ij})$.

3. Results and discussion

Figure 1(a) shows different examples of vortex trajectories. We identify the vortex position with that of its centre, i.e., the cell with vorticity $n_\alpha = 1$ (see equation (8)).

Thus, during the motion, the vortex position acquires discretized values. We define a cell-average velocity $v(x)$ as $1/T_n$, where T_n is the time that the vortex spends in cell n. It is trivially related to the instantaneous velocity, $v_i(x)$, $v(x) = \langle v_i(t)\rangle_n$, where

$$\langle v_i(t)\rangle_n = [1/(t_{n+1} - t_n)] \int_{t_n}^{t_{n+1}} v_i(t)\ \mathrm{d}t$$

(t_α is the time at which the vortex enters cell α).

Remarkably, for all of the trajectories the velocity v remains constant along the ladder, except in the cells near the border, where the vortex accelerates. This behaviour occurs for all values of i_{ext} and $\lambda_\perp$. This fact is connected to the vortex extension: studies on larger 2D arrays [7] reveal that the vortex accelerates when it is at distances from the border of the order of its radius. In the ladder the small transversal length (a, the lattice spacing) constrains the vortex to occupy a restricted extension (see figure 1(b)).

We remark that a constant velocity of transmission, together with a strong vortex localization, is a very desirable characteristic for the development of cryoelectronics devices.

The dependence of v on the external current i_{dc} and the penetration depth $\lambda_\perp$ is shown in figure 2. From figure 2(a) we conclude that, if one is interested in the controlled propagation of one single vortex, the relevant range of i_{dc}-values is $[i_d, i_c]$, where $i_d = 0.458 \pm 0.002$ is the depinning current at zero magnetic field. Above the critical current $i_c = 1$, once the laminar flux of the current has been distorted by a perturbation (e.g. the presence of a vortex), one observes the periodic creation of new vortices. This hinders the ladder operation as a 1D transmission line of single bits. Figure 2(b) shows, for different bias currents, how the velocity decreases as $\lambda_\perp$ is reduced.

The Gibbs energy of a phase configuration in a Josephson junction array is given by

$$U = \sum_i i_{ext;i}\phi_i - \sum_{ij} \cos(\phi - \phi_j - A_{ij})$$

(if screening effects are not negligible, it is necessary to add the magnetic energy term $\frac{1}{2} i_{ij} L_{ij;kl} i_{kl}$). In the case of one single vortex, U can be decomposed into five terms: $U(x) = U_0(x) + U_i(x) + U_c + U_{pot}(x) + U_{f_0}(x)$. They give an account, respectively, of the vortex energy in zero external magnetic field, the vortex interaction with the bias current, the core energy (half of the energy required to create a vortex–antivortex pair $U_c = \pi^2/2$), the energy due to the periodic structure of the ladder, and the interaction with the external magnetic field. For simplicity, we consider the contribution of the self-field included in U_0. In our case ($f = 0$) the relevant terms are U_i, U_0 and U_{pot}. Their expressions, calculated in a 2D array in the $\lambda_\perp \to \infty$ limit (no screening), are [8]

$$U_0(x) = \pi \ln\left(\frac{2L}{\pi} \cos\left(\frac{\pi x}{L}\right)\right) \tag{9}$$

$$U_i(x) = -2\pi i \left(x + \frac{L}{2}\right) \tag{10}$$

and

$$U_{pot}(x) = -\frac{1}{2} E_B \cos(2\pi x). \tag{11}$$

All of these energies are given in terms of $E_J = I_c\Phi_0/(2\pi)$. L is the perpendicular dimension of the array (with respect to that of the bias current), and E_B is the energy

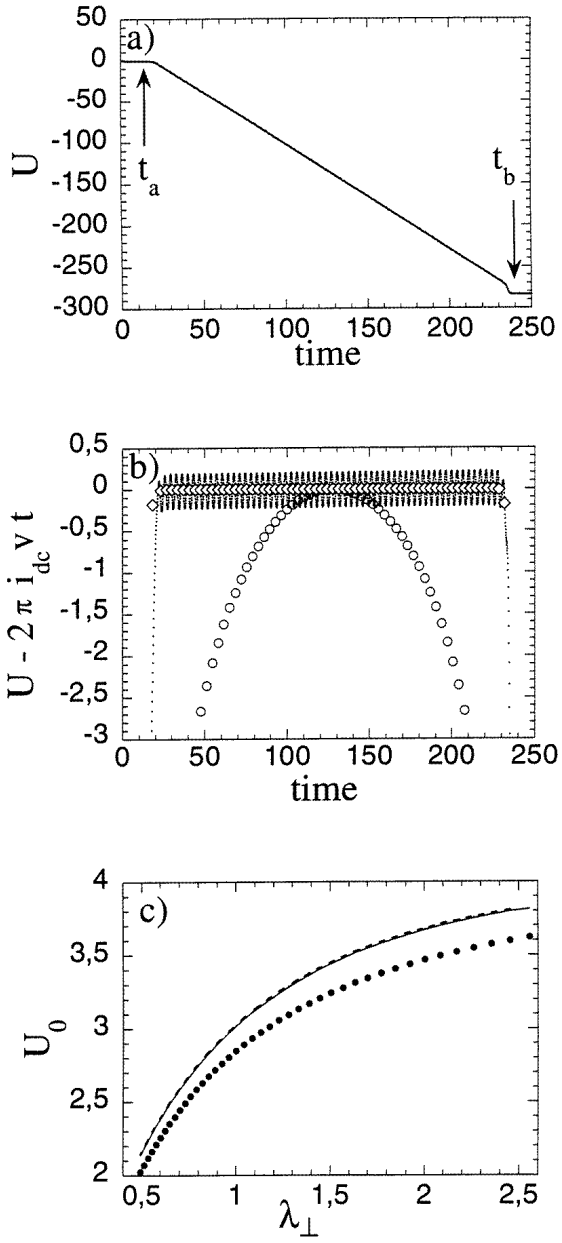

Figure 3. (a) $U(t)$ during the motion of a vortex in a 128-cell ladder, with $i_{dc} = 0.7$, $\lambda_\perp = \infty$. At t_a the vortex is created and begins to move; at t_b it gets to the border of the ladder and disappears. $U(t)$ can be fitted with the straight line for $2\pi i_{dc}x$ or, equivalently, $2\pi i_{dc}vt$. U is given in units of $E_J = I_c\Phi_0/(2\pi)$. (b) $U - 2\pi i_{dc}x$ versus t. The figure clearly shows the U-oscillations as the vortex moves from one cell to the next. The fit to the large 2D expression for U_0 is not so satisfactory: we compare $U - 2\pi i_{dc}x(t)$ (black dots) with the value of U for a static vortex as a function of x (rhombs) and the large 2D expression $\pi \ln((2L/\pi)\cos(\pi x/L))$ (open circles). The three curves have been shifted so as to have the same value at $x = 0$. (c) $U_0(x)$ as a function of $\lambda_\perp$: $U_0(0)$ (black dots), $U_0(1)$ (continuous line) and $U_0(2)$ (discontinuous line). The curves have been shifted so that the absolute minimum of the energy ($U = -E_J n_{links}$, where n_{links} is the number of links in the array) is now $U = 0$.

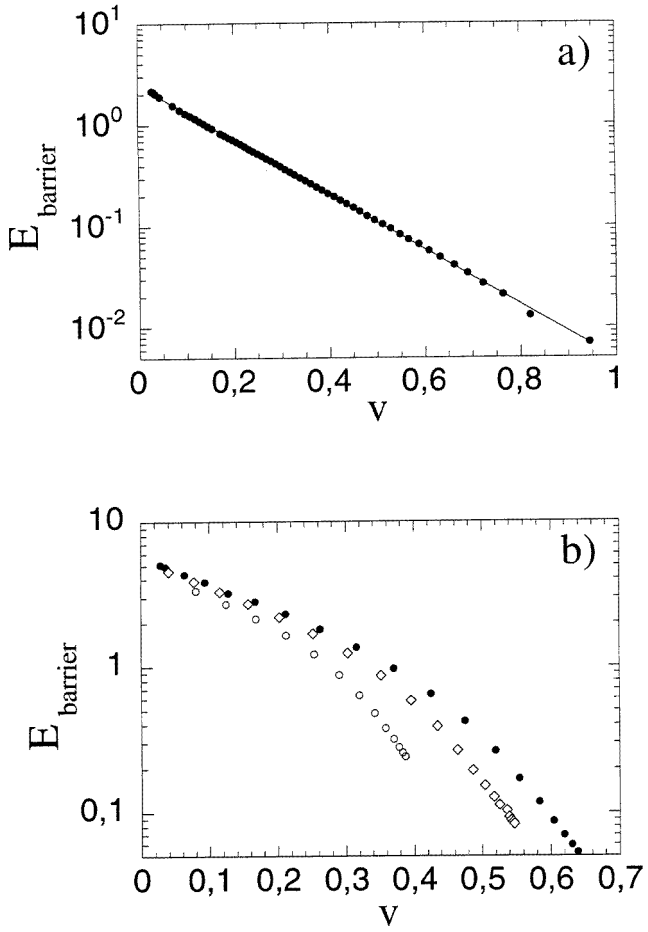

Figure 4. E_B versus v. (a) We neglect inductance effects ($\lambda = \infty$) and make i_{dc} vary. The resulting E_B is an exponential function of v: $E_B = \alpha \exp(-\beta v)$ (in this case, $\alpha \approx 2.5$ and $\beta \approx 2\pi$). (b) E_B versus v for different values of $\lambda_\perp$. We compare the curves obtained with different bias currents: $i_{dc} = 0.95$ (black dots), $i_{dc} = 0.90$ (rhombs) and $i_{dc} = 0.80$ (open circles).

barrier that the vortex must overcome when passing from one cell to the adjacent one. We take the origin, $x = 0$, at the central plaquette of the array.

U_i can be nicely fitted to equation (10), as shown in figure 3(a). In order to study the other components, we subtract $2\pi i_{dc} x$ from U (figure 3(b)). The curve shows a periodic component, which can be directly related to $U_{pot}(x)$.

In a ladder the vortex extension is restricted to a small number of cells. Thus the vortex is not sensitive to border effects unless it is in the vicinity of the ladder edge. This explains the spatial distribution of $U_0(x)$: it is flat inside the ladder and increments at a distance from the border of $2a$–$3a$. The screening field does not qualitatively modify this behaviour: it just produces a shift of the whole energy curve plus an reduction of the $U(x)$-slope near the border (figure 3(c)). This distribution is quite different from that observed for large 2D arrays [7] (the comparison with $U_0(x)$ in the case of infinite penetration depth is made; see again figure 3(b)).

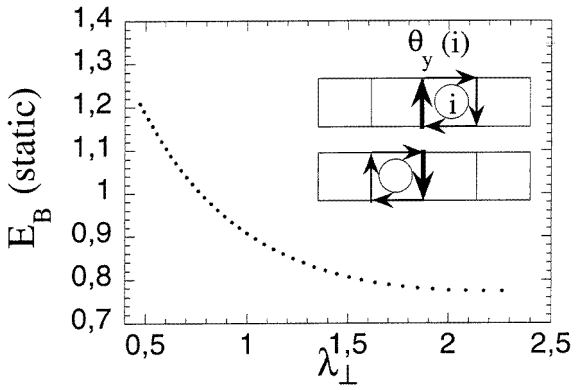

Figure 5. E_B(static) versus $\lambda_\perp$. In the inset we show the current distribution around a vortex when it is in cells i and $i-1$. Note that the values of the vertical current $i_y(i)$ when the vortex is in cell i and in cell $i-1$ are of the same modulus and opposed sign.

From $U_{pot}(x)$ we can obtain E_B in a straightforward way. Figure 4 shows the dependence of E_B on i_{dc} and $\lambda_\perp$. In the limit of infinite penetration depth $\lambda_\perp \to \infty$ (no screening effects) E_B fits very well to an exponential dependence on the velocity v (figure 4(a)). The effect of the self-field is taken into account in figure 4(b). We point out that the extrapolated E_B-value at $v = 0$ is not unique for the different curves: it depends on i_{dc}. We have checked this point as follows: E_B is a smooth function of $\exp(-v)$, and can be fitted to a second-order polynomial; from this fit it is possible to extrapolate E_B in the $v \to 0$ limit.

The values of E_B that we report are quite different from those obtained for a static vortex in large 2D arrays. In particular, for an infinite penetration depth it has been found that $E_B(\text{static}) = 0.2$ [11]; Phillips *et al* have generalized this result taking into account the screening effects: the energy barrier grows as $\lambda_\perp$ decreases, and for example $E_B(\text{static}, \lambda_\perp = 1) \approx 0.4$ [12]. In figure 5 we report the energy barrier of a ladder in the static case. The figure suggests that the restricted vortex extension imposed by the ladder causes an increasing of the static energy barrier. This is defined as $E_B(\text{static}) = E(l) - E(p)$, where $E(p)$ and $E(l)$ are, respectively, the energies of a vortex centred in a plaquette and in a link. In order to calculate E_p we start from the (ϕ_i, A_{ij}) configuration corresponding to the presence of a vortex in the ladder and let the parameter $\lambda_\perp$ vary. The absolute value of the upper and lower horizontal current of the cell with vorticity 1 increases with $\lambda_\perp$, up to its maximum value $i_x = 1$. At this point any small change in $\lambda_\perp$ cannot be sustained by an increase of the currents and the vortex structure becomes unstable. In the case of zero external field, this occurs at $\lambda_{\perp c} = 1.812 \pm 0.018$ [9]. Within a range of $\lambda_\perp$-values above $\lambda_{\perp c}$, the vortex, though unstable, is still maintained. $E(l)$ is obtained by fixing the gauge-invariant phase of the central vertical link to $\pi/2$ and letting the configuration relax with this constraint. This choice of $\phi_y(0)$ is due to the symmetry of the vortex shape: the values of the vertical current $i_y(i)$ (see the inset of figure 5) when the vortex is in cell i and in cell $i-1$ are of the same modulus and opposed sign. Thus there is an intermediate moment when $i_y = 0$, and thus the gauge-invariant phase along the link is $\phi_y = 0$.

The difference between the dynamical and static values of the barrier energy can be qualitatively explained as follows. While the vortex is moving, the phase configuration does not have time to relax, and thus the energy is greater than that of a static vortex. In

addition, there is an extra contribution to the energy, i.e. that supplied by the external current (the supplied power is $\sum_i i_i(\text{ext})\ \mathrm{d}\phi_i/\mathrm{d}t$). The Josephson energy, the externally supplied energy and the magnetic energy have their maxima when the vortex is located between two cells. Thus their contributions to E_B are added.

If the junction capacitance is negligible (the vortex mass is zero), the force balance during the propagation process is

$$\frac{\partial U(x)}{\partial x} = -\eta_0 v(x) \tag{12}$$

where η_0 is the adimensional damping coefficient [10] $\eta = \eta_0 \Phi_0^2/(2a^2R)$. η_0 is a function of both i_{dc} and $\lambda_\perp$, and can be easily computed from figure 2 in the following way: inside a ladder (see figure 3) $\eta_0 v(x)$ is given by a constant value $2\pi i_{dc}$ (coming from U_i) plus an oscillating term $\pi E_B \sin(2\pi x)$. From equation (12) we can deduce the value of $\eta_0 v_i(t)$, where $v_i(t)$ is the instantaneous velocity. As $v(x) = \langle v_i(t)\rangle_n = 2\pi i_{dc}$, $\eta_0 v(x)$ remains constant while the vortex propagates inside the ladder. Its value is given by

$$\eta_0(i_{dc}, \lambda_\perp) = \frac{2\pi i_{dc}}{v(i_{dc}, \lambda_\perp)}. \tag{13}$$

4. Conclusions

In conclusion we have studied in detail the vortex transmission in a ladder of superconducting junctions. In particular, dynamical variables such as the velocity, v, the damping coefficient, η_0, and the dynamical energy barrier, E_B, have been worked out as functions of the bias current, the magnetic penetration depth and the vortex position. v and E_B are shown to be respectively an increasing and a decreasing function of i_{dc} and $\lambda_\perp$.

Inside the ladder, the instantaneous vortex velocity $v_i(x)$ is composed of a constant term plus a sinusoidal component, due to the motion from cell to cell; we can define a cell-average velocity which remains constant throughout. At 2–3 plaquettes from the border, the vortex suddenly accelerates.

We remark that the study of the single-vortex dynamics, besides its interest as a theoretical problem, is relevant for practical implementations of arrays of Josephson junctions. In particular, most cryoelectronics devices are based upon the use of vortices or antivortices as signals carrying information quanta.

We stress that variables such as v or E_B are measurable quantities, so our results could be experimentally checked by means of, e.g., low-temperature scanning electron microscopy (LTSEM) [13]. This technique allows one to measure time-averaged voltage fluctuations (ΔV) with a high spatial resolution. $\Delta V(x)$ can be related to the vortex/antivortex velocity at cell x. On the other hand, from the spatial variation of the velocity $v(x)$ it is possible to extract the value of E_B.

Acknowledgment

J C Ciria acknowledges a post-doctoral grant provided by the MEC (Spain).

References

[1] For a recent review on the state-of-the-art see, e.g.,
Giovannella C and Tinkham M (ed) 1995 *Macroscopic Quantum Phenomena and Coherence in Superconducting Networks* (Singapore: World Scientific)

[2] See, e.g.,
Pedersen N F and Ustinov A V 1995 *Supercond. Sci. Technol.* **8** 389
Nordman J E 1995 *Supercond. Sci. Technol.* **8** 681
[3] See, e.g., for SQFL
Likharev K K and Semenov V K 1991 *IEEE Trans. Appl. Supercond.* **1** 3
Nakajima K, Mizusawa H, Sugahara H and Sawada Y 1991 *IEEE Trans. Appl. Supercond.* **1** 29
and see for NN
Mizugaki Y, Nakajima K, Sawada Y and Yamashita T 1993 *Appl. Phys. Lett.* **62** 762
and for transistors
Berman D, van der Zant H S J, Orlando T P and Delin K A 1994 *IEEE Trans. Appl. Supercond.* **4** 1051
and finally for photofluxonic detectors
Kadin A M 1990 *J. Appl. Phys.* **68** 5741
Cai Y, Leath P L and Yu Z 1994 *Phys. Rev.* **49** 4015
Pacetti P, Ciria J C and Giovannella C 1994 *Nuovo Cimento* D **16** 2039
Ciria J C, Pacetti P, Paoluzi L and Giovannella C 1995 *Nucl. Instrum. Methods* **370** 128
[4] Mon K K and Teitel S 1989 *Phys. Rev. Lett.* **62** 673
Chung J S, Lee K H and Stroud D 1989 *Phys. Rev.* B **40** 6570
[5] Nuvoli A, Giannelli A, Ciria J C and Giovannella C 1994 *Nuovo Cimento* **16** 2045
[6] Orlando T P, Mooij J E and van der Zant H S J 1991 *Phys. Rev.* B **43** 10 218
[7] Ciria J C and Giovannella C 1996 in preparation
[8] See, e.g.,
van der Zant H S J, Rijken H A and Mooij J E 1983 *J. Low Temp. Phys.* **27** 150
[9] Mazo J J and Ciria J C 1996 *Phys. Rev.* B at press
[10] Rzchowski M S, Benz S P, Tinkham M and Lobb C J 1990 *Phys. Rev.* B **42** 2041
[11] Lobb C J, Abraham D W and Tinkham M 1983 *Phys. Rev.* B **27** 150
[12] Phillips J R, van der Zant H S J, White J and Orlando T P 1993 *Phys. Rev.* B **47** 5219
[13] Lachenmann S G, Doderer T, Hoffmann D, Huebener R P, Booi P A A and Benz S P 1994 *Phys. Rev.* B **50** 3158